Dielectric and Viscoelastic Study of Entanglement Dynamics: A Review of Recent Findings

Hiroshi Watanabe, Yumi Matsumiya, Tadashi Inoue*

Institute for Chemical Research, Kyoto University, Uji, Kyoto 611-0011, Japan

Summary: This article gives a review of the results of recent dielectric and viscoelastic studies for entangled binary blends of linear *cis*-polyisoprenes to explain the current understanding of the equilibrium entanglement dynamics on the basis of the molecular picture of dynamic tube dilation (DTD). Comparison of dielectric and viscoelastic properties reveals that the full-DTD picture regarding the relaxed portions of the chains as a solvent fails for the high molecular weight component chain in the blends at intermediate times. This failure is related to insufficient constraint release (CR) equilibration of the entanglement segments of this chain. A partial-DTD picture properly considering this CR equilibration successfully describes the linear relaxation behavior of the blends. The dielectric and viscoelastic properties of PI under fast flow, being affected by the flow-activated CR/DTD mechanism, are also presented in order to demonstrate the usefulness of the comparison of these properties in both equilibrium and non-equilibrium states.

Keywords: chain; viscoelastic properties

Introduction

Theoretical as well as experimental efforts have been made for the entanglement dynamics of flexible polymer chains.[1-3] For linear chains, the tube model of Doi and Edwards represents the entanglement constraint as an impenetrable tube in which a focused chain exhibits curvilinear diffusion referred to as *reptation*.[3] Although the Doi-Edwards (DE) model offered a remarkable framework relating all slow dynamic properties to the reptative motion of the chain, the model did not describe experimental data quantitatively because it assumed that the chain has a constant contour length and the tube constraining this chain is fixed in space. After the DE model, theoretical refinements have been made to remove these assumptions, and the current tube model for linear chains incorporates the contour length fluctuation (CLF) and tube motion in addition to reptation. The CLF process is well described on the basis of the curvilinear Rouse dynamics,[3] while the modeling of the tube motion requires further efforts, as explained below.

The tube motion has been modeled with two different (but related) approaches. In the first approach, the entanglement segment of the molecular weight M_e and an equilibrium

 DOI: 10.1002/masy.200551005

size a ($\propto M_e^{1/2}$) is utilized as a motional unit of a focused chain.[4] This segment is allowed to hop over a distance a in a direction lateral to the tube axis when a tube forming chain (surrounding chain) diffuses away. This hopping process, being equivalent to local motion of the tube and referred to as a local *constraint release* (CR) process, is accumulated over the whole contour of the chain to result in the Rouse-like global CR relaxation. This CR mechanism is considered to compete with the reptation and CLF mechanisms to determine the relaxation behavior of actual chains. Description of this competition requires full analysis of longitudinal as well as lateral motion of the entanglement segments.[1,5]

In the second approach, a focus is placed on the length scale $a'(t)$ of the lateral CR displacement of the entanglement segments: $a'(t)$ increases with increasing time scale t, and successive $\beta(t)$ ($= \{a'(t)\}^2/a^2$) segments are mutually equilibrated through their CR motion in this time scale thereby behaving as a larger, coarse-grained segment. Then, the chain effectively moves in a dilated tube of a diameter a' ($> a$) without exhibiting lateral hopping out of this tube, and the coarse-grained segment behaves as the unit of this motion. In this molecular picture of *dynamic tube dilation* (DTD), the chain exhibits just the longitudinal motion due to reptation and CLF along the tube dilating with t.[1,2,6]

In the DTD picture, we need to specify $\beta(t)$ (or $a'(t)$) as a function of t. $\beta(t)$ is unequivocally determined by the local CR rate. However, in most of the current DTD models, the relaxed portions of the chains are regarded as a non-entangling "solvent", and a system having the fraction of the unrelaxed portion $\varphi'(t)$ (= survival fraction of the dilated tube) at time t is treated as a polymer solution of a concentration φ'. Then, without detailed analysis of the CR process, $\beta(t)$ and $a'(t)$ are expressed in terms of $\varphi'(t)$ as

$$\beta(t) = \{\varphi'(t)\}^{-d}, \quad a'(t) = \{\varphi'(t)\}^{-d/2}a \tag{1}$$

Here, d (= 1-1.3) is the dilation exponent. This $a'(t)$ is the maximum diameter of the dilated tube for a given value of $\varphi'(t)$, and the molecular picture utilizing this $a'(t)$ assumes full dilation of the tube (*full-DTD*) in any time scale.

The full-DTD models describe the linear viscoelastic property of various systems considerably well.[6-13] However, this result does not necessarily mean that the actual chain moves in a way assumed in the models, because the viscoelastic property reflects just a particular aspect of the chain dynamics, a decay of the *isochronal* orientational anisotropy

of the chain. It is important to examine the other properties that reflect a different aspect of the chain dynamics. From this point of view, we recently examined dielectric property of entangled *cis*-polyisoprenes (PI).[14-22] The PI chains have electrical dipoles (type-A dipoles) parallel along their backbone, and the orientational correlation of the chain *at two separate times* (say 0 and t) is detected as a slow dielectric relaxation. Thus, comparison of the dielectric and viscoelastic properties enables us to resolve details of the chain dynamics.[1,18] Indeed, this comparison revealed a failure of the full-DTD picture for binary blends of linear PI chains[14,20,21] as well as for monodisperse star PI chains.[15-17]

This article gives a review of the results of this comparison for PI/PI blends[20,21] to explain the current molecular picture of the entanglement dynamics at equilibrium. A brief summary is also given for the dielectric/viscoelastic properties of monodisperse PI under fast flow[22] to demonstrate the usefulness of the comparison of these properties in investigation of the chain dynamics in the non-equilibrium steady state.

Equilibrium Dynamics of PI/PI Blends

Overview of viscoelastic and dielectric relaxation

For binary blends of high-M and low-M monodisperse PI chains having the molecular weights $M_2 = 308 \times 10^3$ and $M_1 = 21.4 \times 10^3$, Figure 1a shows the normalized linear viscoelastic relaxation function $\mu(t)$ (= $G(t)/G_N$ with G_N being the entanglement plateau modulus) at 40°C. For comparison, the $\mu(t)$ data are also shown for the pure component chains. In the experiments, the storage and loss moduli $G'(\omega)$ and $G''(\omega)$ were measured as a function of the angular frequency ω and the $\mu(t)$ data were evaluated from these $G'(\omega)$ and $G''(\omega)$ data.[20] Both of M_2 and M_1 are well above M_e for bulk PI (= 5×10^3), and the high-M chain (L308) is entangled with the low-M chain (L21) in all blends examined. The high-M chains are mutually entangled when their volume fraction υ_2 exceeds 0.1.

For these blends, Figure 1b shows the normalized dielectric relaxation function $\Phi(t)$ evaluated from the dielectric loss $\varepsilon''(\omega)$ and dynamic dielectric constant $\varepsilon'(\omega)$.[20] Since the PI chains have the type-A dipoles parallel along the backbone, the global motion of the high-M and low-M chains is clearly detected as the two-step dielectric relaxation. This dielectric behavior is qualitatively similar to the two-step viscoelastic relaxation behavior seen in Figure 1a. However, the intensity of the slow relaxation of the high-M chain decreases with decreasing υ_2 more strongly for the viscoelastic μ than for the dielectric Φ.

Quantitatively, the terminal viscoelastic relaxation intensity of the high-M chain is proportional to $\upsilon_2^{2.3}$ and υ_2 in the concentrated and dilute regimes (for $\upsilon_2 \geq 0.1$ and $\upsilon_2 \leq 0.01$), respectively, while the dielectric relaxation intensity of this chain is proportional to υ_2 in the entire range of υ_2.[20] This difference emerges because the same motion of the chain is differently reflected in the viscoelastic and dielectric properties, as explained later in more details.

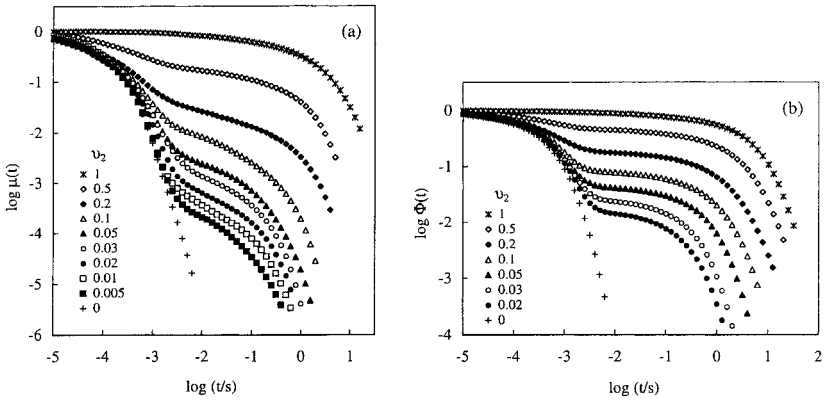

Figure 1. Normalized viscoelastic and dielectric relaxation functions $\mu(t)$ and $\Phi(t)$ of the L308/L21 blends at 40°C. υ_2 is the volume fraction of the high-M chain (L308).

The viscoelastic relaxation time of the high-M chain $\tau_{2,G}$, defined as a product of the zero-shear viscosity and steady state compliance of this chain, was evaluated from the G' and G'' data of the blends.[20] The dielectric relaxation time of the high-M chain $\tau_{2,\varepsilon}$ was similarly evaluated from the ε' and ε'' data.[20] The dielectric $\tau_{1,\varepsilon}$ of the low-M chain was evaluated as a reciprocal of the ε'' peak frequency in the high-ω regime.[20] Figure 2 shows plots of these relaxation times against the volume fraction υ_2 of the high-M chain.

For small $\upsilon_2 \leq 0.1$, the dielectric $\tau_{1,\varepsilon}$ of the low-M chain in the blends (filled triangles) coincides with $\tau_{1,\varepsilon}$ of this chain in its bulk monodisperse state (horizontal dashed line). For large $\upsilon_2 \geq 0.2$, $\tau_{1,\varepsilon}$ increases moderately because of a moderate increase of the entanglement lifetime for the low-M chain due to the entanglement with concentrated high-M chains.[1]

Now, we turn our attention to $\tau_{2,\varepsilon}$ and $\tau_{2,G}$ of the high-M chain (filled and unfilled circles). $\tau_{2,\varepsilon}$ is larger than $\tau_{2,G}$ by a factor $\cong 2$ but the υ_2 dependence is quite similar for these times, confirming that the dielectric relaxation detects the global motion of this chain.

In a range of $\upsilon_2 \geq 0.1$ where the high-M chains are mutually entangled, $\tau_{2,\varepsilon}$ and $\tau_{2,G}$ increase with increasing υ_2 in a way similar to that observed for entangled solutions of the high-M chains in an *iso*-frictional state. This result indicates that the low-M chain behaves as a simple solvent for the mutually entangled high-M chains in long time scales. Indeed, the full-DTD picture with the dilation exponent $d \cong 1.3$ is valid for these high-M chains in long time scales, as shown later in Figure 4. In contrast, for small $\upsilon_2 \leq 0.01$, $\tau_{2,G}$ is independent to υ_2; see Figure 2. Since M_2 is much larger than M_1 in the blends examined, this υ_2-independent $\tau_{2,G}$ (= 0.08 s) is assigned as the Rouse-like constraint release (CR) time $\tau_{CR,G}^{\ 0}$ for the dilute high-M chains entangled only with the low-M chains.

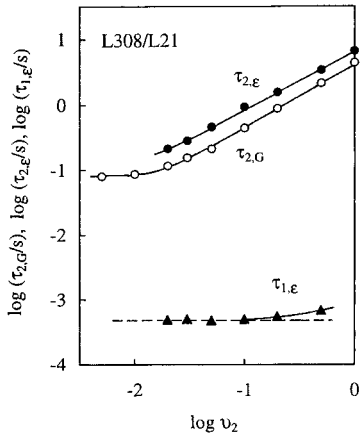

Figure 2. Dependence of the relaxation times of the high-M and low-M chains in the L308/L21 blends at 40°C on the volume fraction of the high-M chain. Reproduced from the paper by Watanabe et al.[20]

Difference between viscoelastic and dielectric relaxation processes

As explained for Figure 1, the terminal viscoelastic intensity of the high-M chain is proportional to $\upsilon_2^{2.3}$ and υ_2 in the concentrated and dilute regimes, respectively, while the dielectric intensity of this chain is proportional to υ_2 in both regimes.[20] This difference reflects a difference in the DTD effects on the viscoelastic and dielectric properties.

In order to clarify this difference of the DTD effects, we first focus on the microscopic expression of the stress. In the polymeric liquids with $M >> M_e$, the entanglement segments naturally behave as the stress-sustaining units in long time scales, and the deviatoric part of the stress tensor **S** is expressed in terms of the bond vector **u** of these segment.[1-3] If the tube dilates to the diameter $a' = \beta^{1/2}a$, successive β entanglement

segments are mutually equilibrated to behave as a coarse-grained (enlarged) segment, and **S** can be also expressed in terms of the bond vector (end-to-end vector) **r** of these enlarged segments.[1] Thus, whenever the tube dilates, **S** is expressed in a dual form,[1]

$$\mathbf{S} = 3G_N\left[\frac{<\mathbf{uu}>}{a^2} - \frac{trace<\mathbf{uu}>}{3a^2}\mathbf{I}\right]$$
$$= 3G_N\left[\frac{<\mathbf{rr}>}{\beta^2 a^2} - \frac{trace<\mathbf{rr}>}{3\beta^2 a^2}\mathbf{I}\right] \quad (2)$$

Here, **I** denotes the unit tensor. (The front factor, "3", changes a little according to our choice of the molecular expression of G_N.[1,2] However, this minor change does not affect the discussion in this paper.) The tensors (dyadic) **uu** and **rr** appearing in Eq.(2) represent the orientational anisotropy/stretching of the entanglement segment and enlarged segment, respectively, and <...> represents the average over all segments.

The above duality of the stress expression is an essential feature of DTD. Under a small shear in the linear viscoelastic regime, the chain conformation deviates from the Gaussian conformation only slightly and the entanglement segments/enlarged segments are negligibly stretched to have $<u^2> = a^2$ and $<r^2> = \beta a^2$. In this regime, the deviatoric stress tensor given by Eq.(2) is fully characterized with its shear component $\sigma = 3G_N<\tilde{u}_x\tilde{u}_y> = 3G_N<\tilde{r}_x\tilde{r}_y>/\beta$, where the shear and shear-gradient directions are chosen as the x- and y-directions, respectively, and $\tilde{u}_\xi$ and $\tilde{r}_\xi$ represent the ξ component of the normalized bond vectors $\tilde{\mathbf{u}} = \mathbf{u}/|\mathbf{u}|$ and $\tilde{\mathbf{r}} = \mathbf{r}/|\mathbf{r}|$. As noted from this expression of σ, the orientational anisotropy in the presence of DTD is smaller for the entanglement segments than for the enlarged segments ($<\tilde{u}_x\tilde{u}_y> < <\tilde{r}_x\tilde{r}_y>$) because of the CR motion of the former segments within the dilated tube. This fact means that the internally equilibrated, enlarged segments behave as the *independently* stress-sustaining units whenever the tube dilates. (The mutually equilibrated entanglement segments *cooperatively* sustain the stress.)

During the stress relaxation under step strain in the presence of DTD, the initial orientation of any entanglement segment partly relaxes due to its CR motion within the dilated tube. In contrast, the initial orientation is preserved for the enlarged segments in a surviving portion of the dilated tube. Thus, the normalized viscoelastic relaxation function is expressed as $\mu(t) = \varphi'(t)/\beta(t)$ where $\varphi'(t)$ is the fraction of the enlarged segments in that

portion (= survival fraction of the dilated tube) and $\beta(t)$ is the CR-equilibration number of the entanglement segments at time t.[1,6] The factor of $1/\beta(t)$ represents the decrease of the total number of the enlarged segments, the independently stress-sustaining units during the DTD process.

Furthermore, if the relaxed portion of the chains behaves as a solvent and the full-DTD picture is valid, $\beta(t)$ scales as $\{\varphi'(t)\}^{-d}$ (Eq.(1)) and $\mu(t)$ is simply written as[1,2,6]

$$\mu(t) = \{\varphi'(t)\}^{1+d} \quad (\text{with } d \cong 1.3 \text{ for PI/PI}^{[20]}) \tag{3}$$

For our PI/PI blends having $M_2 >> M_1$, the low-M chain relaxes much faster than the high-M chain, and $\varphi'(t)$ at long t is essentially proportional to the high-M chain content υ_2. Then, $\mu(t)$ for large υ_2 (≥ 0.1) scales as $\upsilon_2^{2.3}$ at long t, as observed experimentally.[20]

Now, we turn our attention to the normalized dielectric relaxation function $\Phi(t)$ at equilibrium. In general, $\Phi(t)$ detects fluctuation of the microscopic polarization $P_E(t)$ in the direction of the electric field and coincides with the auto-correlation function of $P_E(t)$.[23,24] For the PI chains having the type-A dipoles, $P_E(t)$ is proportional to a component of the end-to-end vector in this direction, $R_E(t)$. At equilibrium, all directions are equivalent and the auto-correlation function of R_E (and P_E) coincides with that of the end-to-end vector **R**. Thus, $\Phi(t)$ of the PI/PI blends is written as[18,20]

$$\Phi(t) = (1-\upsilon_2)\Phi_1(t) + \upsilon_2\Phi_2(t) \tag{4}$$

with

$$\Phi_j(t) = \frac{<\mathbf{R}_j(t)\bullet\mathbf{R}_j(0)>}{a^2N_j}, \quad a^2N_j = <R_j^2> \tag{5}$$

Here, the subscript j specifies the chain component (j = 1 and 2 for low-M and high-M chains), and N_j is the number of the entanglement segments per chain j.

The dielectric $\Phi_j(t)$ is essentially insensitive to the DTD mechanism,[20,21] as can be noted for a model case of a type-A network strand having fixed ends and being entangled with matrix chains: The strand segments are CR-equilibrated on the matrix diffusion to exhibit a decay of their stress due to the DTD mechanism, but this CR/DTD process activates no dielectric relaxation because the end-to-end vector of the strand does not change with t. Because of this insensitivity, the terminal dielectric intensity of the high-M chain scales as υ_2 in the entire range of υ_2 even in the presence of the DTD mechanism, as observed experimentally.[20]

Test of full-DTD picture

A key quantity in the test of the DTD picture is the survival fraction of the tube for the component chain j, $\varphi_j'(t)$. This fraction can be evaluated from the dielectric $\Phi_j(t)$ data of the chain j (obtained by separating the $\Phi(t)$ data of the blends (Figure 1b) into contributions from the component chains.[20])

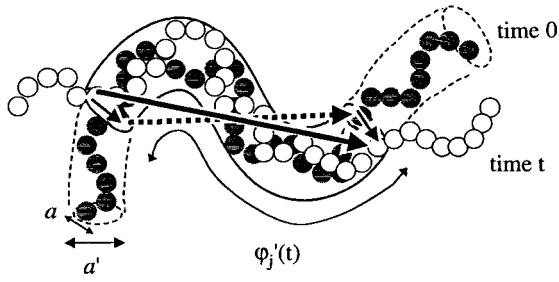

Figure 3. Schematic illustration of the component chain j constrained in the dilated tube.

Figure 3 schematically shows the conformation of the chain j composed of N_j entanglement segments of the size a. The unfilled and filled circles indicate these segments at times t and 0, respectively. A fraction $\varphi_j'(t)$ of the segments at time t is constrained in a surviving portion of the dilated tube of the diameter a'. In this situation, successive $(a'/a)^2$ entanglement segments are coarse-grained into an enlarged segment of the size a'.

The normalized dielectric relaxation function $\Phi_j(t)$ of the chain j is given by the auto-correlation function of its end-to-end vector; cf. Eq.(5). Since the entanglement segments at time t located outside the surviving portion of the dilated tube have no memory of their initial orientation, $\Phi_j(t)$ is contributed only from the $\varphi_j'N_j$ segments remaining in this portion and given by $\langle \mathbf{R}_{in}(t)\cdot\mathbf{R}_{in}(0)\rangle/a^2N_j$. Here, $\mathbf{R}_{in}(t)$ and $\mathbf{R}_{in}(0)$, shown with the thick solid and dotted arrows in Figure 3, represent the end-to-end vector defined for the these $\varphi_j'N_j$ segments at times t and 0, the respectively. $\mathbf{R}_{in}(t)$ coincides with a sum $\mathbf{R}_{in}(0) + \mathbf{D} + \mathbf{D}'$, where $\mathbf{D}$ and $\mathbf{D}'$ (shown with the thin solid arrows) are the displacements of the chain at the two edges of the surviving portion of the dilated tube. Thus we find $\Phi_j(t) = [\langle\{\mathbf{R}_{in}(0)\}^2\rangle + \langle\mathbf{R}_{in}(0)\cdot\mathbf{D}\rangle + \langle\mathbf{R}_{in}(0)\cdot\mathbf{D}'\rangle]/a^2N_j$. $\langle\{\mathbf{R}_{in}(0)\}^2\rangle$ is the mean-square end-to-end distance of the sequence of $\varphi_j'N_j$ entanglement segments and given by $a^2\varphi_j'N_j$, and an

analysis of Gaussian conformation of the chain[19] indicates $\langle \mathbf{R}_{in}(0)\cdot\mathbf{D}\rangle = \langle \mathbf{R}_{in}(0)\cdot\mathbf{D}'\rangle = -(a'-a)^2/8$. From these results, we obtain[19,21]

$$\Phi_j(t) = \varphi_j'(t) - \frac{1}{4N_j}[\{a'(t)/a\} - 1]^2 \qquad (6)$$

Furthermore, for the case of full-DTD, Eq.(1) relates the dilated tube diameter $a'(t)$ to the tube survival fraction $\varphi'(t)$ averaged for the high-M and low-M chains ($\varphi'(t) = (1-\upsilon_2)\varphi_1'(t) + \upsilon_2\varphi_2'(t)$). For this case, Eq.(6) is reduced to

$$\Phi_j(t) = \varphi_j'(t) - \frac{1}{4N_j}[\{\varphi'(t)\}^{-d/2} - 1]^2 \qquad (7)$$

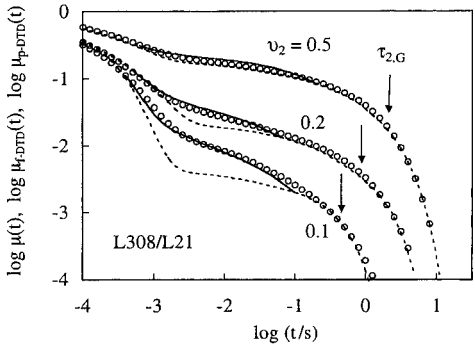

Figure 4. Comparison of μ data of the L308/L21 blends (circles) with $\mu_{f\text{-}DTD}$ (dotted curve) and $\mu_{p\text{-}DTD}$ (solid curve) for the full-DTD and partial-DTD processes. The arrows indicate the terminal viscoelastic relaxation time of the high-M chain (L308). Reproduced from the paper by Watanabe et al.[21]

Now, the full-DTD molecular picture can be straightforwardly tested. The tube survival fractions $\varphi_j'(t)$ are evaluated from the dielectric $\Phi_j(t)$ data with the aid of Eq.(7), and the viscoelastic relaxation function for the full-DTD process, $\mu_{f\text{-}DTD}(t)$, is simply calculated from $\varphi'(t)$ ($= (1-\upsilon_2)\varphi_1'(t) + \upsilon_2\varphi_2'(t)$) through Eq.(3). For the bends containing mutually entangled high-M chains ($\upsilon_2 \geq 0.1$), Figure 4 compares this $\mu_{f\text{-}DTD}$ (dotted curves) with the μ data (circles). A good agreement of $\mu_{f\text{-}DTD}$ and μ data is noted at long and short t where the high-M and low-M chains exhibit respective terminal relaxation. Thus, the full-DTD picture is valid at those t. However, at intermediate t where the low-M chain has fully relaxed but the high-M chain exhibits just moderate relaxation, $\mu_{f\text{-}DTD}$ is considerably smaller than the μ data and this picture fails for the high-M chains. More significant failure was noted for mutually non-entangled high-M chain ($\upsilon_2 < 0.1$).[21] The origin of the

failure is discussed below in relation to the constraint release (CR), the pre-requisite for DTD.

CR-equilibration and partial-DTD

Since the tube dynamically dilates as a result of accumulation of the local CR hopping of the entanglement segments, the number of these segments in an enlarged (dilated) segment, β_{DTD}, cannot exceed the number β_{CR} of the entanglement segments that can be CR-equilibrated in a given time scale. Thus, a comparison of these numbers is very helpful for specifying the criterion for the validity of the full-DTD picture.

For evaluation of β_{CR}, we focus on the pure Rouse-like CR behavior observed for the high-M chain with $\upsilon_2 \leq 0.01$. The relaxation time of this chain, $\tau_{2,G} = 0.08$ s (Figure 2), is assigned as the viscoelastic CR time $\tau_{CR,G}^{\circ}$ of the *dilute* high-M chains entangled only with the low-M chains. The terminal CR-equilibration time $\tau_{CR,1}^{(j)}$ of the chain j for arbitrary υ_2 was estimated from this $\tau_{CR,G}^{\circ}$, and $\tau_{CR,1}^{(j)}$ was utilized to formulate a *hypothetical* stress decay function $\Theta_{j,CR}(t)$ for the chain j due only to the CR mechanism:[21]

$$\Theta_{j,CR}(t) = \frac{1}{N_j}\sum_{p=1}^{N_j} \exp\left(-\frac{t}{\tau_{CR,p}^{(j)}}\right) \tag{8}$$

Here, $\tau_{CR,p}^{(j)}$ is the characteristic time of p-th Rouse-CR mode of the chain j evaluated from $\tau_{CR,1}^{(j)}$ with the aid of the modified Rouse scheme.[21] This $\Theta_{j,CR}(t)$ specifies a fractional decrease of the stress due only to the CR-equilibration. Thus, the CR-equilibration number for the chain j is given by $\beta_{j,CR}(t) = 1/\Theta_{j,CR}(t)$.

For the blends with $\upsilon_2 \geq 0.1$, Figure 5 compares this $\beta_{j,CR}(t)$ and the equilibration number assumed in the full-DTD picture,[21] $\beta_{f\text{-}DTD}(t) = \{\varphi'(t)\}^{-1.3}$ (Eq.(1) with $d = 1.3$) where φ' was evaluated from the dielectric data through Eq.(7). Since $\beta_{f\text{-}DTD}$ and $\beta_{j,CR}$ are essentially integer, a difference between $\beta_{f\text{-}DTD}$ and $\beta_{j,CR}$ is interpreted to be significant only when $\left|\beta_{f\text{-}DTD} - \beta_{j,CR}\right| > 1$. With this criterion, we note in Figure 5 that $\beta_{f\text{-}DTD}$ (solid curve) does not exceed $\beta_{1,CR}$ of the low-M chain (circles) in the entire range of $t \leq \tau_{1,G}$ ($\tau_{1,G}$ = terminal viscoelastic relaxation time of this chain).[21] Thus, for the low-M chain in its terminal regime, the CR mechanism allows the tube to dilate up to the full-DTD diameter $a'(t) = \{\varphi'(t)\}^{-d/2}a$. Similarly, for the high-M chain, $\beta_{f\text{-}DTD}$ is smaller than $\beta_{2,CR}$

(squares) at long $t \cong \tau_{2,G}$ so that the full-DTD picture holds in its terminal regime. However, at intermediate t, $\beta_{f\text{-}DTD}$ is considerably larger than $\beta_{2,CR}$ for the high-M chain with $\upsilon_2 = 0.2$ and 0.1. This result means that the CR mechanism does not allow the tube to dilate to the full-DTD diameter $a'(t)$ at those t. This insufficient dilation results in the failure of the full-DTD picture seen at intermediate t (Figure 4). Milner et al.[12] compared their full-DTD model and viscoelastic data to find a similar failure for star/linear blends.

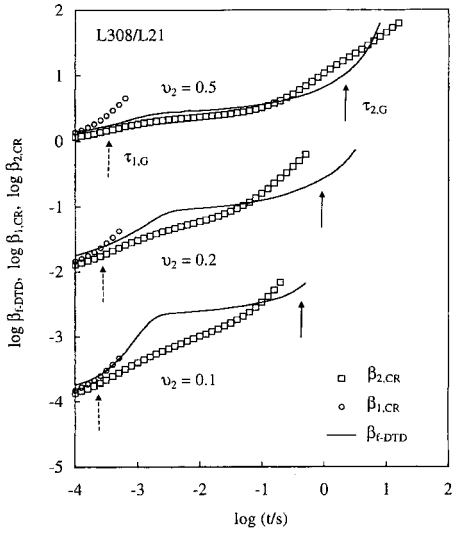

Figure 5. Comparison of the CR-equilibration number $\beta_{j,CR}(t)$ of the entanglement segments of chain j in the L308/L21 blends with the number $\beta_{f\text{-}DTD}(t)$ of these segments in the enlarged segment assumed in the full-DTD picture. These numbers are double-logarithmically plotted against time t. To avoid heavy overlapping of the plots, the plots for $\upsilon_2 = 0.2$ and 0.1 are shifted vertically by factors of -2 and -4, respectively. Reproduced from the paper by Watanabe et al.[21]

In a range of t where the CR-determined diameter $a''(t) = \{\beta_{j,CR}(t)\}^{1/2}a$ is smaller than $a'(t)$ and the full-DTD picture fails, the tube should still dilate to the diameter $a''(t)$. Thus, we can formulate the maximum possible number $\beta_j^*(t)$ of the equilibrated entanglement segments of the chain j for a given $\varphi'(t)$ value as[21]

$$\beta_j^*(t) = \beta_{j,CR}(t) \quad \text{at } t \text{ where } \beta_{j,CR}(t) < \beta_{f\text{-}DTD}(t) \tag{9a}$$

$$\beta_j^*(t) = \beta_{f\text{-}DTD}(t) \text{ at } t \text{ where } \beta_{j,CR}(t) > \beta_{f\text{-}DTD}(t) \tag{9b}$$

Utilizing these $\beta_j^*(t)$ (evaluated from the β data shown in Figure 5), we can introduce a *partial-DTD* picture in which the tube for the chain j dilates to the maximum possible diameter $a^*(t) = \{\beta_j^*(t)\}^{1/2}a$. For this picture, the viscoelastic relaxation function is formulated as[21]

$$\mu_{\text{p-DTD}}(t) = \frac{(1-\upsilon_2)\varphi_1'(t)}{\beta_1^*(t)} + \frac{\upsilon_2\varphi_2'(t)}{\beta_2^*(t)} \tag{10}$$

where the factors $1/\beta_j^*(t)$ represent the stress decay due to partial-DTD.

The partial-DTD relaxation function $\mu_{\text{p-DTD}}(t)$ was evaluated from the $\beta_j^*(t)$ and $\varphi_j'(t)$ data: $\varphi_j'(t)$ was dielectrically determined through Eq.(6) with $a'(t)$ therein being replaced by $a^*(t) = \{\beta_j^*(t)\}^{1/2}a$.[21] For the blends with $\upsilon_2 \geq 0.1$, $\mu_{\text{p-DTD}}(t)$ thus evaluated is shown with the solid curves in Figure 4. In a range of t where the solid curves are not shown, the full-DTD picture is valid and $\mu_{\text{p-DTD}}(t)$ coincides with $\mu_{\text{f-DTD}}(t)$ shown with the dotted curve. The $\mu_{\text{p-DTD}}$ agrees well with the μ data (circles) in the entire range of t. Similar agreement was found also for the blends with $\upsilon_2 < 0.1$.[21] These results demonstrate the usefulness of the partial-DTD picture, i.e., the DTD picture that incorporates the dilated tube diameter being consistent with the CR mechanism.

Non-equilibrium Entanglement Dynamics Under Fast Flow

Overview of rheo-dielectric behavior in Non-Newtonian regime

One of the most prominent rheological features of entangled polymer chains is the non-Newtonian thinning behavior of the steady state viscosity η and first normal stress coefficient Ψ_1 under fast shear flow, $\eta \propto \dot{\gamma}^{-\alpha}$ and $\Psi_1 \propto \dot{\gamma}^{-\alpha'}$ with $\alpha \cong 0.8$ and $\alpha' \cong 1.6$ in a range of shear rate $\dot{\gamma}$ between the equilibrium terminal relaxation frequency $1/\tau_G$ and the Rouse frequency $1/\tau_R$ ($>> 1/\tau_G$).[1,2] In this range of $\dot{\gamma}$, the chains are largely oriented but not significantly stretched, and the above power-law type thinning behavior is exclusively attributed to this flow-induced orientation.[1,2]

For such shear-oriented but unstretched chains, the stress-optical rule allows us to express Ψ_1 and the second normal stress coefficient Ψ_2 in terms of the normalized bond vector of the entanglement segments, $\tilde{\mathbf{u}} = \mathbf{u}/|\mathbf{u}|$ with $|\mathbf{u}| = a$ for the unstretched segments.[1-3,22] From this expression together with a relationship between Ψ_1 and Ψ_2 experimentally observed in a wide range of normalized shear rate $\dot{\gamma}\tau_G$, $\Psi_2 \cong -0.1\,\Psi_1$,[25-27]

we can estimate second moment averages of $\tilde{\mathbf{u}}$ as[22]

$$<\tilde{u}_x^2>=\frac{1}{3}\left[1+\frac{1.9\dot{\gamma}^2\Psi_1}{3G_N}\right],\quad <\tilde{u}_y^2>=\frac{1}{3}\left[1-\frac{1.1\dot{\gamma}^2\Psi_1}{3G_N}\right] \qquad (11)$$

Here, $\tilde{u}_x$ and $\tilde{u}_y$ are the components of $\tilde{\mathbf{u}}$ in the shear and shear-gradient directions (x- and y-directions).

For an entangled solution of monodisperse linear PI ($M = 1190 \times 10^3$, $C = 15$ wt%) in a moderately good, non-entangling solvent, an oligomeric butadiene ($M = 2 \times 10^3$), $<\tilde{u}_x^2>$ and $<\tilde{u}_y^2>$ were evaluated from the Ψ_1 data through Eq.(11).[22] In Figure 6a, these second-moment averages are plotted against the normalized shear rate $\dot{\gamma}\tau_G$. $<\tilde{u}_x^2>$ and $<\tilde{u}_y^2>$ increases and decreases, respectively, from their equilibrium values (= 1/3) on the increase of $\dot{\gamma} > 1/\tau_G$, quantifying the shear-induced orientation of the entanglement segments of the PI chain.

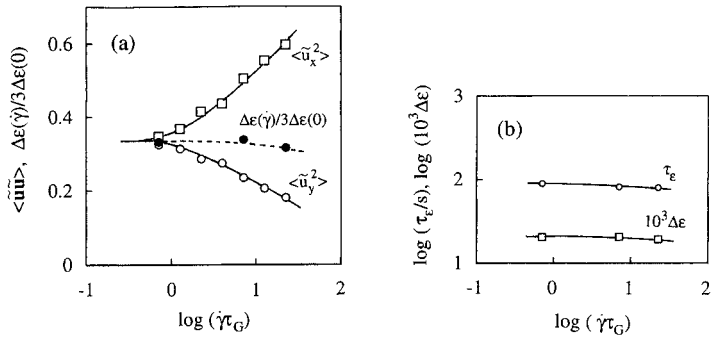

Figure 6. Second moment averages of normalized bond vector, $<\tilde{\mathbf{u}}\tilde{\mathbf{u}}>$, dielectric intensity ratio, $\Delta\varepsilon(\dot{\gamma})/3\Delta\varepsilon(0)$, dielectric intensity, $\Delta\varepsilon(\dot{\gamma})$, and dielectric relaxation time, $\tau_\varepsilon(\dot{\gamma})$, measured for an entangled solution of monodisperse linear PI ($M = 1190 \times 10^3$, $C = 15$ wt%) in an oligomeric butadiene at 30°C. The data are plotted against the normalized shear rate $\dot{\gamma}\tau_G$. Reproduced from the paper by Watanabe et al.[22]

The shear-induced orientation observed for various entangled systems is weaker than that predicted from the fixed tube model,[1-3] as was the case also for the entangled PI solution examined in Figure 6a.[22] Thus, the model has been refined by introducing a flow-activated constraint release referred to as the *convective constraint release* (CCR):[28-30] CCR reduces the orientation and weakens the $\dot{\gamma}$ dependence of the η and Ψ_1, as first

noticed by Ianniruberto and Marrucci.[28] In fact, the η and Ψ_1 data are well described by the CCR models of Mead-Larson-Doi[29] and Milner-McLeish-Likhtman.[30]

Thus, the CCR model appears to describe a particular aspect of the chain conformation under flow, the orientational anisotropy of *individual* segments monitored through the η and Ψ_1 data. However, the other aspect of the conformation, the orientational cross-correlation of *neighboring* segments, is not sensitively resolved in these data, as noted from a fact that the same anisotropy can be achieved for parallel and anti-parallel alignments of neighboring segments. This cross-correlation can be rheo-dielectrically tested, as demonstrated in a recent study.[22] In this test, guarded cone-plate electrodes are mounted on a rheometer and the dielectric and rheological responses under shear are simultaneously measured.[22,31,32] The gap angle between the truncated cone and plate is small (< 3 degrees) and the electric field is uniformly applied in the shear gradient direction.[22,31,32]

The rheo-dielectric tests have been made for various systems[22,31-37] including the entangled PI solution examined in Figure 6a. In Figure 6b, the dielectric intensity $\Delta\varepsilon$ and relaxation time τ_ε of the PI chain in this solution under flow are plotted against the normalized rate $\dot{\gamma}\tau_G$. The dielectric behavior is only weakly affected by the flow up to $\dot{\gamma} \cong 20/\tau_G$, possibly due to the flow-induced orientational cross-correlation of neighboring entanglement segments of the PI chain. For further discussion of this cross-correlation, a relationship between the dielectric property and chain conformation under fast shear is examined in the next section. Then, this relationship is utilized to discuss the flow-activated cross-correlation.

Microscopic expression of dielectric property under fast shear

At equilibrium, the unnormalized dielectric relaxation function $F(t)$ is rigorously related to a component $P_y(t)$ of microscopic polarization in the direction of the electric field (= y direction):[23,24]

$$F(t) = \langle P_y(t)P_y(0)\rangle = \Delta\varepsilon\,\Phi(t) \quad \text{for } t \geq 0 \tag{12}$$

For the linear PI chains, $P_y(t)$ is proportional to the y component of the end-to-end vector, $R_y(t)$, and the dielectric intensity $\Delta\varepsilon$ and the normalized dielectric relaxation function $\Phi(t)$ (= 1 at t = 0) appearing in Eq.(12) are written as[18]

$$\Delta\varepsilon = K_\varepsilon \nu < R_y^2 > \text{ and } \Phi(t) = \frac{< R_y(t) R_y(0) >}{< R_y^2 >} \qquad (13)$$

Here, K_ε is a constant determined by the magnitude of the type-A dipoles and ν is the number of the chains per unit volume. (Eq.(13) is equivalent to Eq.(5).)

Under the flow examined in Figure 6, the PI chains are largely oriented but not stretched to have an equilibrium contour length. For these chains, we may assume validity of Eqs.(12) and (13) *if* the local equilibrium is achieved under the flow. Recently, Masubuchi et al.[38] conducted molecular simulations (Naples simulation) based on the primitive chain network model[39] to test this assumption. This model faithfully considers the force balance at the entanglement nodes and includes all known relaxation mechanisms. The Naples simulation satisfactorily reproduces viscoelastic data of entangled chains.[38-41]

In the test, Masubuchi et al.[38] put positive and negative charges at two ends of the entangled linear chain and simulated a macroscopic polarization $\mathbf{P}_m(t)$ induced by a small electric field **E**. These charges were equivalent to summed-up type-A dipoles of the PI chain. Thus, the simulation well mimicked actual rheo-dielectric experiments and gave the macroscopic dielectric relaxation function defined in terms of $\mathbf{P}_m(t)$ and **E**. This function was found to agree with the microscopic function $\Phi(t)$ defined by Eq.(13) even at $\dot{\gamma} = 10/\tau_G$, demonstrating the validity of Eqs.(12) and (13) under fast shear.[38] This result lends support to the following molecular analysis based on Eqs.(12) and (13).

If the entanglement segments have no isochronal cross-correlation, Eq.(13) gives $\Delta\varepsilon = K_\varepsilon \nu N a^2 < \tilde{u}_y^2 >$ with N being the number of the segments per chain. This is the case at equilibrium (where $< \tilde{u}_y^2 > = 1/3$), and $\Delta\varepsilon$ in the zero-shear limit is written as $\Delta\varepsilon(0) = K_\varepsilon \nu N a^2/3$. In contrast, under fast shear, the CCR mechanism should equilibrate successive entanglement segments to raise the cross-correlation and effectively dilate the tube. For this CCR-DTD occurring over β_{flow} entanglement segments, Eq.(13) gives $\Delta\varepsilon(\dot{\gamma}) = K_\varepsilon \nu N a^2 [< \tilde{u}_y^2 > + (\beta_{flow} - 1) < \tilde{u}_y \tilde{u}_y' >]$, where $\tilde{u}_y$ and $\tilde{u}_y'$ are the y components of $\tilde{\mathbf{u}}$ of the cross-correlated entanglement segments and the average $< \tilde{u}_y \tilde{u}_y' >$ is taken for all pairs for these segments. Then, the $\Delta\varepsilon(\dot{\gamma})/3\Delta\varepsilon(0)$ ratio is related to $< \tilde{u}_y^2 >$ and $< \tilde{u}_y \tilde{u}_y' >$ as[22]

$$\frac{\Delta\varepsilon(\dot{\gamma})}{3\Delta\varepsilon(0)} = <\tilde{u}_y^{\,2}> + (\beta_{\text{flow}} - 1) <\tilde{u}_y \tilde{u}_y'> \qquad (14)$$

Eq.(14) allows us to examine the chain dimension under flow through the dielectric data.

Orientational cross-correlation under fast shear

For the PI solution examined in Figure 6, we evaluated the $\Delta\varepsilon(\dot{\gamma})/3\Delta\varepsilon(0)$ ratio from the $\Delta\varepsilon$ data. The results are shown in Figure 6a with the filled circles. This ratio decreases with increasing $\dot{\gamma}$ much more weakly compared to $<\tilde{u}_y^{\,2}>$ (unfilled circles), and the difference $\Delta\varepsilon(\dot{\gamma})/3\Delta\varepsilon(0) - <\tilde{u}_y^{\,2}> = (\beta_{\text{flow}} - 1) <\tilde{u}_y \tilde{u}_y'>$ quantifies the CCR-induced cross-correlation of the entanglement segments under fast shear (cf. Eq.(14)).

With the CCR mechanism, successive β_{flow} entanglement segments should be coarse-grained into an enlarged (dilated) segment and their stress is expressed in the dual form, Eq.(2). This expression specifies a relationship between the orientational anisotropies of the bond vectors **u** and **r** of the entanglement segment and enlarged segment (cf. <**uu**> and <**rr**> terms in Eq.(2)). From this relationship and an independent analysis of the configuration of the entanglement segments (modeled as freely jointed rods[42-44]), we found that CCR-equilibrated entanglement segments are not stretched but have a very strong orientational cross-correlation (almost parallel alignment characterized with $<\tilde{u}_y \tilde{u}_y'> \cong <\tilde{u}_y^{\,2}>$) thereby highly stretching the enlarged segment.[22] Then, Eq.(14) is reduced to

$$\frac{\Delta\varepsilon(\dot{\gamma})}{3\Delta\varepsilon(0)} \cong \beta_{\text{flow}} <\tilde{u}_y^{\,2}> \qquad (15)$$

We utilized Eq.(15) to estimate β_{flow} from the $<\tilde{u}_y^{\,2}>$ and $\Delta\varepsilon(\dot{\gamma})/3\Delta\varepsilon(0)$ data (Figure 6). For the linear PI solutions with $M = 1190 \times 10^3$ and $C = 10$ and 15 wt%,[22] Figure 7 shows plots of β_{flow} against the normalized shear rate $\dot{\gamma}\tau_G$. β_{flow} increases to $\cong 1.8$ with increasing $\dot{\gamma}$ up to $20/\tau_G$. Note that only a small number ($\cong 1.8$) of the neighboring segments are CCR-equilibrated even at the highest $\dot{\gamma}$ examined but this mild CCR-DTD effect is sufficient to give the weak $\dot{\gamma}$ dependence of $\Delta\varepsilon(\dot{\gamma})$ (and $<R_y^2>$) seen in Figure 6b.

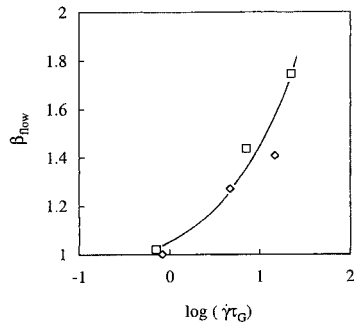

Figure 7. CCR-equilibrated number β_{flow} of the entanglement segments in the entangled linear PI solutions with $M = 1190 \times 10^3$ (squares and diamonds for $C = 15$ and 10 wt%). β_{flow} is plotted against the normalized shear rate $\dot{\gamma}\tau_G$. Reproduced from the paper by Watanabe et al.[22]

Here, a comment needs to be added for the β_{flow} value. The thermal constraint release (simply abbreviated as CR in this paper) occurs for monodisperse high-M PI at equilibrium to give a considerably large equilibration number, $\beta^* \cong 7$ at $t \cong \tau_G$.[21] The thermal CR would occur also under the fast flow, and the net number of the entanglement segments equilibrated through the thermal and convective CR would be close to a product $\beta_{flow}\beta^*$.[22] Since the tube for the monodisperse PI at equilibrium is considerably dilated at long t, the dilation due to CCR-DTD under flow appears to be limited to a moderate level thereby giving a rather small β_{flow} value. Theoretical studies are desired for this combination of the thermal and convective CR mechanisms.

Chain motion under fast shear

As seen in Figure 6b, the large scale motion of the entangled linear PI chain characterized with the dielectric τ_ε is just weakly accelerated with increasing shear rate up to $\dot{\gamma} = 20/\tau_G$. This behavior is to be related to the CCR-DTD mechanism, but no detailed analysis based on the current CCR models has been made for τ_ε.

For this weak acceleration, it is informative to examine results of the Naples simulation by Masubuchi et al.[38] In their simulation scheme, the creation of the new entanglement is affected by the force balance at the existing entanglement nodes and the predicted $\dot{\gamma}$ dependence of τ_ε is weaker than that of the viscosity η, which is in harmony with the experimental observation.[22]

Masubuchi et al.[38] also demonstrated the importance of the so-called hidden entangled appearance (HEA) mechanism proposed by Ianniruberto and Marrucci.[45] In this mechanism, a chains that was neighboring to but not entangled with a focused chain before occurrence of CCR is explicitly entangled with the focused chain after CCR, and this creation of new entanglement affects the conformations of these chains. Masubuchi et al.[38] incorporated the HEA mechanism into their Naples simulation and showed that the HEA mechanism further weakens the $\dot{\gamma}$ dependence of τ_ε without giving detectable effects on the viscoelastic properties. The η and τ_ε obtained from the Naples + HEA simulation are shown in Figure 8. The calculated $\dot{\gamma}$ dependence is considerably weaker for τ_ε than for η, and the $\dot{\gamma}$ dependence of η is close to the experimental observation. Although the calculated τ_ε decreases with $\dot{\gamma}$ more strongly compared to the τ_ε data (Figure 6b), the result seen in Figure 8 suggests that the HEA mechanism combined with the force balance and CCR plays an important role in the chain dynamics under fast flow.

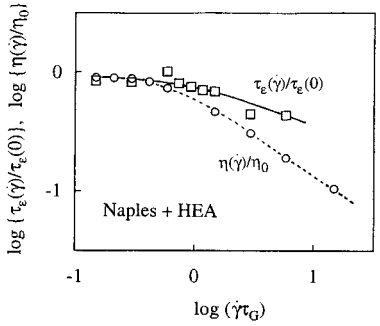

Figure 8. Dielectric relaxation time τ_ε and viscosity η under steady shear simulated with Naples incorporating HEA mechanism. τ_ε and η are normalized by respective zero-shear values and plotted against the normalized shear rate, $\dot{\gamma}\tau_G$. Reproduced from the paper by Masubuchi et al.[38]

Conclusions

The entanglement dynamics was investigated through comparison of the dielectric and viscoelastic properties of linear PI chains having the type-A dipoles. The concept of dynamic tube dilation (DTD) at equilibrium was examined for PI/PI blends. It turned out that the molecular picture of full-DTD fails when the equilibration of the entanglement segments due to the thermal constraint release (CR) does not occur in time over the assumed diameter of the dilated tube. The partial-DTD picture properly considering this

CR-equilibration well describes the equilibrium dynamics of the blends.

In the non-Newtonian regime under fast flow, the dielectric intensity $\Delta\varepsilon$ and relaxation time τ_ε of entangled, monodisperse PI were only weakly dependent on the shear rate $\dot{\gamma}$. This result means that the chain dimension and motion in the shear gradient direction, detected through $\Delta\varepsilon$ and τ_ε, are just slightly affected by the flow. The weak $\dot{\gamma}$ dependence of $\Delta\varepsilon$ is consistent with the concept of convective constraint release (CCR) and CCR-activated DTD. However, the weak $\dot{\gamma}$ dependence of τ_ε suggests the importance of the hidden entangled appearance (HEA) mechanism (a mechanism not fully incorporated in the current CCR models) that is related to the creation of new entanglements after occurrence of CCR-DTD. Further theoretical studies are desirable for the combination of the CCR-DTD and HEA mechanisms.

[1] H. Watanabe, *Prog. Polym. Sci.* **1999**, *24*, 1253.
[2] T. C. B. McLeish, *Adv. Phys.* **2002**, *51*, 1379.
[3] M. Doi, S. F. Edwrads, "*The Theory of Polymer Dynamics*", Clarendon Press, Oxford 1986.
[4] W. W. Graessley, *Adv. Polym. Sci.* **1982**, *47*, 67.
[5] A. E. Likthman, T. C. B. McLeish, *Macromolecules* **2002**, *36*, 6332.
[6] G. J. Marrucci, *Polym. Sci. Polym. Phys. Ed.* **1985**, *23*, 159.
[7] R. C. Ball, T. C. B. McLeish, *Macromolecules* **1989**, *22*, 1911.
[8] S. T. Milner, T. C. B. McLeish, *Macromolecules* **1997**, *30*, 2159.
[9] S. T. Milner, T. C. B. McLeish, *Macromolecules* **1998**, *31*, 7479.
[10] S. T. Milner, T. C. B. McLeish, *Phys. Rev. Lett.* **1998**, *81*, 725.
[11] R. H. Colby, M. Rubinstein, *Macromolecules* **1990**, *23*, 2753.
[12] S. T. Milner, T. C. B. McLeish, R. N. Young, A. Hakiki, J. M. Johnson, *Macromolecules* **1998**, *31*, 9345.
[13] S. J. Park, R. G. Larson, *Macromolecules* **2004**, *27*, 597.
[14] Y. Matsumiya, H. Watanabe, K. Osaki, *Macromolecules* **2000**, *33*, 499.
[15] H. Watanabe, Y. Matsumiya, K. Osaki, *J. Polym. Sci. Part B: Polym. Phys.* **2000**, *38*, 1024.
[16] Y. Matsumiya, H. Watanabe, *Macromolecules* **2001**, *34*, 5702.
[17] H. Watanabe, Y. Matsumiya, T. Inoue, *Macromolecules* **2002**, *35*, 2339.
[18] H. Watanabe, *Macromol. Rapid Commun.* **2001**, *22*, 127.
[19] H. Watanabe, *Korea-Australia Rheol. J.* **2001**, *13*, 205.
[20] H. Watanabe, S. Ishida, Y. Matsumiya, T. Inoue, *Macromolecules* **2004**, *37*, 1937.
[21] H. Watanabe, S. Ishida, Y. Matsumiya, T. Inoue, *Macromolecules* **2004**, *37*, 6619.
[22] H. Watanabe, S. Ishida, and Y, Matsumiya, *Macromolecules* **2002**, *35*, 8802.
[23] R. H. Cole, *J. Chem. Phys.* **1965**, *42*, 637.
[24] E. Riande, E. Saiz, E. "*Dipole Moments and Birefringence of Polymers*", Prentice Hall Press, Englewood Cliffs, New Jersey, 1992.
[25] K. Osaki, S. Kimura, M. Kurata, M., *J. Polym. Sci. Polym. Phys. Ed.* **1981**, *19*, 517.
[26] J. J. Magda, C.S. Lee, S. J. Muller, R. G. Larson, *Macromolecules* **1993**, *26*, 1696.
[27] E. F. Brown, W. R. Burghardt, H. Kahvand, D. C. Venerus, *Rheol. Acta* **1995**, *34*, 221.
[28] G. Ianniruberto, G. Marrucci, G., *J. Non-Newtonian Fluid Mech.* **1996**, *65*, 241.
[29] D. W. Mead, R. G. Larson, M. Doi, *Macromolecules* **1998**, *31*, 7895.
[30] S. T. Milner, T. C. B. McLeish, A. E. Likhtman, *J. Rheol.* **2001**, *45*, 539.
[31] Y. Matsumiya, H. Watanabe, T. Inoue, K. Osaki, M. L. Yao, *Macromolecules* **1998**, *31*, 7973.
[32] H. Watanabe, T. Sato, Y. Matsumiya, T. Inoue, K. Osaki, *Nihon Reoroji Gakkaishi* (*J. Soc. Rheol. Japan*) **1999**, *27*, 121.
[33] H. Watanabe, T. Sato, M. Hirose, K. Osaki, M. L. Yao, *Rheol. Acta* **1998**, *37*, 519.
[34] H. Watanabe, T. Sato, M. Hirose, K. Osaki, M. L. Yao, *Rheol. Acta* **1999**, *38*, 100.
[35] H. Watanabe, Y. Matsumiya, M. Kakiuchi, Y. Aoki, *Nihon Reoroji Gakkaishi* (*J. Soc. Rheol. Japan*) **2001**, *29*, 77.
[36] H. Watanabe, Y. Matsumiya, T. Inoue, *J. Phys. Condensed Matter* **2003**, *15*, S909.
[37] Y. Matsumiya, N. P. Balsara, J. B. Kerr, T. Inoue, H. Watanabe, *Macromolecules* **2004**, *37*, 544.
[38] Y. Masubuchi, H. Watanabe, G. Ianniruberto, F. Greco, G. Marrucci, *Nihon Reoroji Gakkaishi* (*J. Soc. Rheol. Japan*) **2004**, *32*, 197.
[39] Y. Masubuchi, J-I Takimoto, K. Koyama, G. Ianniruberto, G. Marrucci, F. Greco, *J. Chem. Phys.* **2001**, *115*, 4387.
[40] Y. Masubuchi, G. Ianniruberto, G. Marrucci, F. Greco, *J. Chem. Phys.* **2003**, *119*, 6925.
[41] Y. Masubuchi, G. Ianniruberto, G. Marrucci, F. Greco, *Modelling Simul. Mater. Sci. Eng.* **2004**, *12*, S91.
[42] K. Nagai, *J. Phys. Soc. Japan* **1958**, *13*, 928.
[43] C. Hsiung, H. Hsiung, A. Gordus, *J. Chem. Phys.* **1964**, *34*, 535.
[44] H. Yamakawa, "*Modern Theories of Polymer Solutions*", Harper & Row, New York, 1971.
[45] G. Ianniruberto, G. Marrucci, *J. Non-Newtonian Fluid Mech.* **2000**, *95*, 363.